# A Realistic Pelvic Phantom for Electrical Impedance Measurement

**Eoghan Dunne**[1,2]**, Brian McGinley**[1,3]**, Martin O'Halloran**[1,2] **and Emily Porter**[1,2]
[1]Translational Medical Device Lab, National University of Ireland Galway, Galway City, Ireland
[2]Department of Electrical & Electronic Engineering, College of Engineering & Informatics, National University of Ireland Galway, Galway City, Ireland
[3]Department of Computer Science & Applied Physics at Galway-Mayo Institute of Technology, Galway, Ireland.

E-mail: e.dunne13@nuigalway.ie

**Abstract.**

*Objective:* To design and fabricate an anatomically and conductively accurate phantom for electrical impedance studies of non-invasive bladder volume monitoring.

*Approach:* A modular pelvic phantom was designed and fabricated, consisting of a mechanically and conductively stable boundary wall, a background medium, and bladder phantoms. The wall and bladders are made of conductive polyurethane. The background material is an ultrasound gel-based mixture, with conductivity matched to a weighted average of the pelvic cavity organs, bone, muscle and fat. The phantom boundary is developed using a computer tomography model of a male human pelvis. The bladder phantoms were designed to correlate with human bladder dimensions. Electrical impedance measurements of the phantom were recorded, and images produced using six different bladder phantoms and a realistic finite element model.

*Main results*: Five different bladder volumes were successfully imaged using an empty bladder as a reference. The average conductivity index from the reconstructed images showed a strong positive correlation with the bladder phantom volumes.

*Significance:* A conductively and anatomically accurate pelvic phantom was developed for non-invasive bladder volume monitoring using electrical impedance measurements. Several bladders were designed to correlate with actual human bladder volumes, allowing for accurate volume estimation. The conductivity of the phantom is accurate over 50-250 kHz. This phantom can allow: changeable electrode location, contact and size; multi-layer electrodes configurations; increased complexity by addition of other organ or bone phantoms; and electrode movement and deformation. Overall, the pelvic phantom enables greater scope for experimentation and system refinement as a precursor to in-man clinical studies.

**Keywords:** electrical impedance, bladder volume monitoring, realistic pelvic phantom, conductively accurate, urinary bladder

## 1. Introduction

Electrical impedance tomography (EIT) is a low-cost, non-invasive medical imaging technology. This technique involves injecting small alternating electrical currents and measuring the resultant voltages at electrodes on the boundary of an anatomical region, in order to monitor some physiological state or process. Electrical impedance tomography is a particularly useful technology for monitoring fluid and gas changes over time, due to its strong temporal resolution. This medical technology has been employed in the monitoring of lung (Frerichs *et al.*, 2016), perfusion (Frerichs *et al.*, 2002), cardiac (Proença *et al.*, 2016), gastric and intestinal (Mangnall *et al.*, 1987) functions, as well as bladder volume monitoring (BVM) (Leonhardt *et al.*, 2011).

Bladder volume monitoring using electrical impedance (EI) techniques has been studied in simulation (Schlebusch *et al.*, 2014), with simplified tank-based measurements (He *et al.*, 2012; Schlebusch *et al.*, 2014), on animals (Denniston and Baker, 1975; Schlebusch *et al.*, 2014; Zariffa *et al.*, 2016), and on humans (Kim *et al.*, 1998; Leonhardt *et al.*, 2011; Liao and Jaw, 2011; Zariffa *et al.*, 2016, Shin, *et al.*, 2017). Human studies have shown strong correlation of bladder volume with the processed EI data (Leonhardt *et al.*, 2011; Li *et al.*, 2016), highlighting the feasibility of EI to continuously monitor bladder volume in clinical situations. Bladder volume monitoring using EI offers the potential to aid paraplegic patients, those suffering from urological diseases or those who have lost bladder control by alerting the individual/carer before urination. Bladder volume monitoring using EI also has the potential to act as a support tool for children with nocturnal enuresis (Shin, *et al.*, 2017). Therefore, this intervention has the potential to preserve the individual's dignity, aid their quality of life and prevent subsequent medical problems such as urinary tract infections, urinary reflux, or renal failure (Li *et al.*, 2016).

Despite initial success of EI for BVM, full clinical implementation is being hindered by key variables, such as electrode movement, contact impedance, body deformation, and urine conductivity changes. Laboratory experiments have been performed on experimental setups mimicking regions of the human body, called phantoms. Phantoms allow variables to be controlled, which is difficult in clinical experiments. In BVM, cylindrical (Schlebusch *et al.*, 2014) or cuboidal (He *et al.*, 2012) shaped phantoms have been employed to model the pelvic region boundary. The cylindrical tank used by Schlebusch *et al.* (2014) and Li *et al.* (2016) restricted electrode locations to where the electrode holes had been drilled into the tank. The cuboidal agar phantom used by He *et al.* (2012) catered for different electrode locations when 3D imaging a cuboidal bladder phantom. However, the phantom boundary was not anatomically accurate. Investigation of relevant test scenarios prior to clinical testing is key to achieving successful clinical results. Such testing is dependent on the quality and accuracy of the phantom, as well as the variations of experimental parameters that the phantom allows. These experimental parameters include the electrode locations, contacts, sizes, material types, and the number of rings. An in-depth understanding of how the variation of each of these parameters impacts measured impedance data is vital in order to design EI systems that function reliably in real-world scenarios.

Anatomically and conductively accurate phantoms provide enhanced experimentation possibilities, beyond those of the phantoms with simple shape and those that have been used in BVM to date. Electrode parameters may be varied, and in the case of modular phantoms, the internal structures may be changed to add or reduce the complexity of the test scenario. Such realistic phantoms have been employed in EIT previously, in particular, for head (Sperandio *et al.*, 2012) and breast (Murphy *et al.*, 2017) applications. The breast and head phantoms vary in terms of their mechanical and long-term electrical stability, their production method, and whether they are one complete unit or modular (Sperandio *el al.*, 2012; Li *et al.*, 2014; Murphy *et al.*, 2017; Zhang *et al.*, 2017). However, no realistic phantom exists for the pelvic region, limiting the scope of experiments that can be conducted before performing costly in-human testing of BVM applications.

In this paper, we present a realistic modular phantom of the pelvic region. We employ realistic bladder phantoms with dimensions that correlate with actual bladder dimensions. A two-dimensional imaging study of the phantoms is also presented using a realistic first-order finite element mesh. Significantly, this pelvic phantom is both conductively and anatomically accurate, and will allow testing of changeable electrode location, contact, and size; multi-layer electrodes configurations; electrode movement and deformation. The ability to test and assess each of these variables will enable greater scope for experimentation before clinical testing.

This paper is structured as follows: the design choices for the phantom are discussed in section 2, the fabrication of the phantom is presented in section 3, the experimental setup and imaging results are described in section 4, and we discuss the results and conclude in section 5.

## 2. Phantom Design Choices

For this pelvic phantom, we were interested in the region from the navel to beginning of the external genital area, as this is the area relevant for BVM. The pelvic region consists of skin, fat, muscle, bone, the lower spine, and the pelvic cavity organs. An adult bladder rests in the anterior of the pelvic cavity and ascends into the abdomen as the bladder fills (Drake *et al.*, 2015). Using this anatomical information, we collected conductivity data for the tissues of interest from the IT'IS database (Hasgall *et al.*, 2015) over the frequency range of 50-250 kHz. This frequency range encapsulates the majority of frequencies that have been used in BVM to date (Leonhardt *et al.*, 2011; He *et al.*, 2012; Li *et al.*, 2016), and matches the frequency range of the Swisstom Pioneer Set (Swisstom.com, Swisstom AG, Switzerland), which we have employed for EI measurement (section 4).

A modular pelvic phantom design was chosen to maximise the number of possible experimental test scenarios. The modularity allows for various bladder sizes, bladder locations, and control over the complexity of the internal tissues by adding or removing organs, muscle or bone in future experiments. The proposed pelvic phantom is flexible, and therefore will enable testing of small deformations on the boundary, which is difficult to achieve with solid phantoms.

The pelvic phantom can be divided into three individual design components: the outer wall, the internal background material, and the bladder phantoms. The outer wall is mechanically and conductively stable, and holds a gel-based background material. The bladder phantoms are suspended into the background material at the anterior of the pelvic phantom.

In this section, we discuss the design choices for the tissues and the pelvic phantom, including size, shape and conductivity; in the next section we discuss how the phantoms are fabricated.

### *2.1. Design of the Outer Wall*

In the pelvic region, as with elsewhere in the body, skin and subcutaneous fat provide protection for the internal tissues and organs. We wish to mimic this protection layer in the phantom as the outer wall layer. Akkus *et al.* (2012) reported that in 449 adult human subjects, the average thickness of the anterior abdominal subcutaneous adipose tissue was 15.73 mm and skin was 2.35 mm. We used a weighted average of the thicknesses of abdominal subcutaneous adipose tissue and the skin to determine the appropriate conductivity for the outer wall. The target conductivity was calculated to be 0.038 S $m^{-1}$, which was determined by employing subcutaneous fat and skin conductivities from the IT'IS Database (Hasgall *et al.*, 2015).

To obtain the shape of the outer wall, computer tomography scans from the Visible Human Project (Ackerman, 1998) were used to form a 3D surface model (Dunne *et al.*, 2017). The 3D surface model was then scaled by 0.516 to allow for rapid prototyping (3D printing) on a Ultimaker 2 Extended+ (Ultimaker, Geldermalsen, Netherlands). This scale makes the model suitable for use in urinary applications for children using electrical impedance (Shin *et al.*, 2017) and as a near-half scale model of an adult male.

### *2.2. Design of the Internal Background*

The background conductivity of the pelvic phantom was determined by a weighted average of the volume occupied by fat, muscle, the pelvic bone, the femur, the spine, and the pelvic cavity organs (excluding the bladder). The volumes of each tissue were approximated using the male computer tomography scans from the Visible Human Project (Ackerman, 1998). Muscle and fat dominated the weighting, contributing approximately 40 % each to the conductivity. The resulting weighted conductivity was approximately 0.2 S $m^{-1}$.

### *2.3. Design of the Bladder Phantoms*

The bladder consists of a thin muscle and membrane layered wall, and a cavity to store urine (Chambers, 2007). For the design of the bladder phantoms, we discount the conductivity of thin bladder wall and based the conductivity of the bladder phantom on the highly conductive urine. According to the database of Hasgall et al., (2015), the conductivity of the bladder wall is 0.22 ± 0.002 S $m^{-1}$ over the frequency range of 50-250 kHz. This conductivity is similar to the conductivity of the internal background material (0.22 ± 0.001 S $m^{-1}$), ensuring that the assumption is appropriate.

Urine mainly consists of minerals and organic waste (Springhouse, 2002). Notably, the conductivity of the urine varies based on the individual, their health, and their diet (Schlebusch *et al.*, 2014). Literature has, subsequently, reported discrepancies for conductivity values of urine. Specifically, Hasgall's *et al.* (2015) database gives the conductivity of urine as 1.75 S $m^{-1}$ over 1-1000 kHz, Gabriel, *et al.* (2009) reports the urine conductivity on the order of 2 S $m^{-1}$ over 1-1000 kHz, Grimnes and Martinsen (2008) gives the range as 0.5-2.6 S $m^{-1}$, and Schlebusch *et al.* (2014) reported interpatient urine conductivity of 0.59-3.22 S $m^{-1}$ in their study.

The human bladder can be modelled as an ellipsoid. Hirahara *et al.* (2006) recorded axial, coronal, and sagittal diameters of 15 healthy male adult volunteers voiding using 4D Ultrasound. We use a similar

method of determining bladder volumes as Krewer *et al.* (2017) employed in microwave imaging of the bladder, i.e., by fitting a regression line to selected data from the study of Hirahara *et al.* (2006). In this study, however, we use the minimum and maximum data points of the 15 healthy volunteers at each recording instance, rather than using the data from just one patient. For each of the 9 recording instances, the minimum and maximum values were averaged. Linear regression lines were formed relating the axial diameters to the bladder volume, and the coronal and sagittal diameters. Figure 1 illustrates the collected points and regression lines relating the coronal diameter, the sagittal diameter, and the bladder volume to the axial diameter.

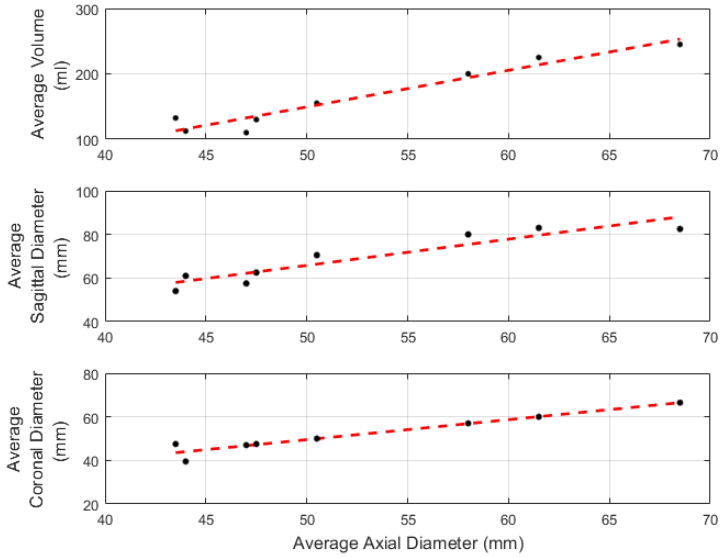


**Figure 1:** Average of the minimum and maximum values of the axial, coronal, sagittal diameters and the bladder volumes at voiding, as reported in Hirahara *et al.*, (2006). Regression lines relating the bladder volume in millilitres (*top graph*), the sagittal (*middle*), and coronal (*bottom*) diameters to the axial diameter were fitted. Using the equations for these lines, the bladder volumes selected could be related to the corresponding diameters. The mean squared errors for each regression line from the top graph to the bottom graph are 13.917 ml, 4.541 mm, and 2.453 mm, respectively.

The axial, coronal, and sagittal diameters associated with bladder volumes of 40, 60, 100, 160, 240, 400 ml were determined using the regression lines shown in figure 1. The volumes were chosen with incremental increases of 20 ml in the first five cases to determine the minimal detectable bladder volumes using EIT. The largest volume was selected based on the findings in Lukacz *et al.*, (2011), which showed an adult bladder functional capacity between 300-400 ml. Thus, the full bladder capacity was taken as 400 ml, to represent the maximum capacity possible and to allow for a strong contrast between empty and full states. The diameters of all bladders were scaled by 0.516 to match the scaling of the outer wall.

## 3. Phantom Fabrication

In this section, we discuss how each layer was fabricated.

### *3.1. Fabrication of the Outer Wall*

A TMM was designed to match the target conductivity of the outer wall (0.038 S $m^{-1}$). The chosen TMM type was conductive polyurethane, originally used in microwave breast cancer imaging studies (Santorelli *et al.*, 2015) and recently introduced to the EIT frequency band (McDermott *et al.*, 2017). Using data collected from McDermott *et al.*, (2017), the composition of 30 % w/w graphite (Graphite powder, general purpose grade from Fisher Scientific, Loughborough, Leics, UK), 5.7 % w/w carbon black (Carbon Black, acetylene 50 % compressed, 99.9 % + from Alfa-Aesar Ward Hill, MA, USA) and the remainder from equal parts of polyurethane precursors (VytaFlex 20 part A and B from Smooth-On, Easton, PA, USA) was chosen as having the best fitting conductivity for the weighted proportions of subcutaneous adipose tissue and skin. The conductivity of the outer wall TMM was measured to be 0.043 ± 0.006 S $m^{-1}$ over 50-250 kHz. The conductive polyurethane TMM was mixed as described in McDermott *et al.*, (2017).

Next, the outer wall was fabricated using the TMM. Two 3-D prints were formed, using the surface models described in Section 2, one to form the boundary of the counter mould using polyurethane and the other to form the inner mould. The base of the counter-mould print was extruded by 1.5 cm to allow a

1.5 cm solid base in the phantom, which enables the phantom to stand independently. The inner mould was printed in four parts to allow for easy insertion and removal during the making of the phantom. The boundary wall of the inner mould was further scaled-down to provide 1 cm thickness between the moulds, which became the thickness of the phantom wall. The thickness is similar to the combined thickness of skin and subcutaneous fat from (Akkus *et al.* 2012) when scaled by 0.516. This thickness of outer wall also provides structural integrity to the phantom to support the fluid contents. Once the mould and counter-mould prints were ready, the counter-mould print was placed into a container of unset polyurethane and left to set for over 24 hours. The counter-mould was then removed. The TMM mixture was then added into the counter-mould. This mixture was plastered to the walls and the four-part inner mould was added. Figure 2 illustrates the prints, the moulds, and the conductive polyurethane setting in the counter-mould.

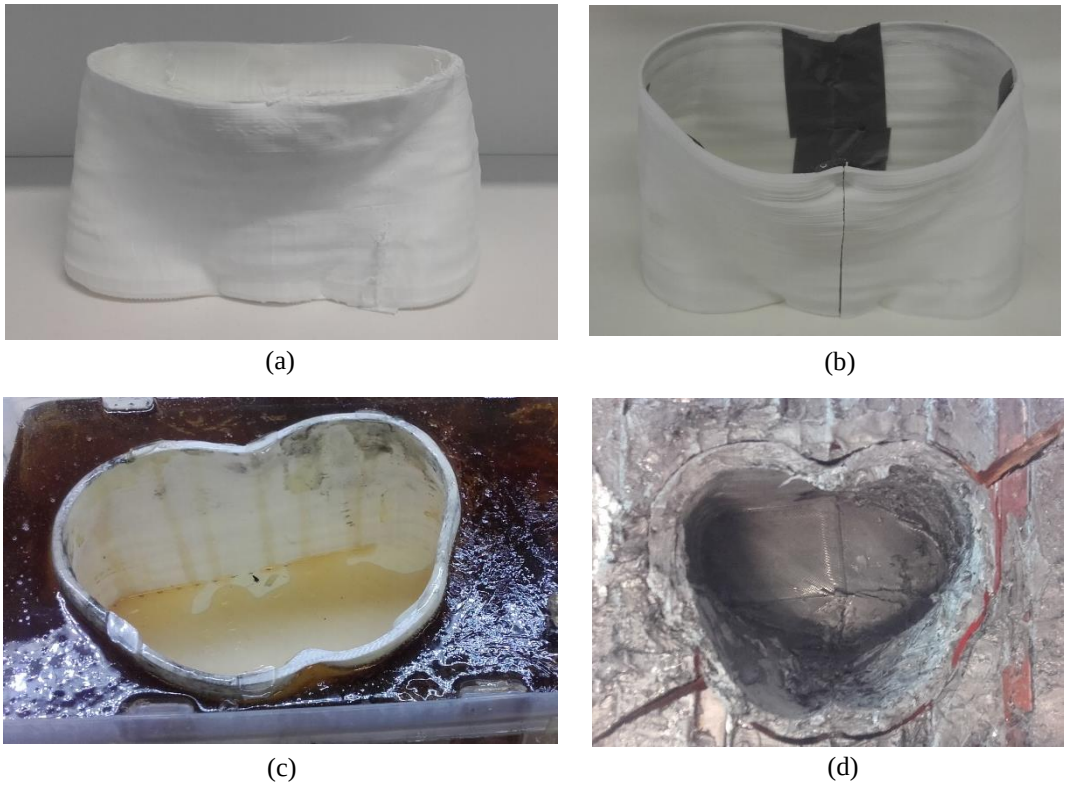

(a) (b)

(c) (d)

**Figure 2:** *(a)* Outer-layer boundary print used to form the polyurethane counter-mould. *(b)* 3D printed four-part inner mould joined together by tape for illustration. *(c)* Polyurethane counter-mould setting. The polyurethane counter-mould is easily dissected in order to remove the print or the casted phantom. *(d)* Casted conductive polyurethane mixture in counter-mould with inner mould removed. Cuts in the counter-mould to aid removal of the phantom can be seen in the bottom-left and top-right corners of this image.

The final outer wall phantom is illustrated in figure 3. The pelvic phantom is 19.5 cm in width, 13.3 cm in depth, and 11.2 cm in height. The phantom has a maximum horizontal circumference is 53.2 cm and is water-tight. The phantom includes the navel and the groove that runs along the lower back.

(a) (b)

**Figure 3:** *(a)* Frontal-view of the outer wall of the pelvic phantom, with a 1 cm solid wall and 1.5 cm solid base. A printed scale is given where each notch marks 1 cm. *(b)* Profile-view of the outer wall phantom.

### *3.2. Fabrication of the Internal Background*

To achieve the target conductivity of 0.2 S $m^{-1}$ for the internal background, an ultrasound gel-based medium was chosen. This gel has mechanically favourable properties, allowing the bladder phantoms to be easily changed. Further, the gel is more viscous than saline, thus, reducing the possibility of small movements of the bladder phantoms due to external forces.

To adjust the conductivity of the chosen TMM, ultrasound gel (product no. 33279, Gima, Italy), to that of the desired target conductivity (0.2 S $m^{-1}$), milligrams of sodium chloride (purity ≥ 99 %, product no. s5886, Sigma-Aldrich, Missouri, United States) were added to ultrasound gel to increase the conductivity. The Keysight E4990A Impedance Analyzer with the Keysight 16452A Liquid Test Fixture (Keysight.com, Keysight Technologies, California, United States) was employed to measure the conductivity of the solution. This fixture uses the parallel plate method to measure the equivalent parallel capacitance and resistance of the solution, which were then converted into dielectric properties using the data processing guidelines detailed in the operational and service manual of the 16452A Liquid Test Fixture (Keysight Technologies, 2017). Stray capacitance was also accounted for. Each measurement was repeated three times for each of several candidate solutions and averaged.

The best fit for the desired weighted background conductivity was a solution of 0.11 % w/w of NaCl in ultrasound gel. The mean conductivity of this solution over 50-250 kHz was measured to be 0.22 ± 0.001 S $m^{-1}$. The conductivity and relative permittivity curves of pure ultrasound gel and the selected ultrasound gel NaCl solution over the frequency range of 1-2000 kHz are given in figure 4.

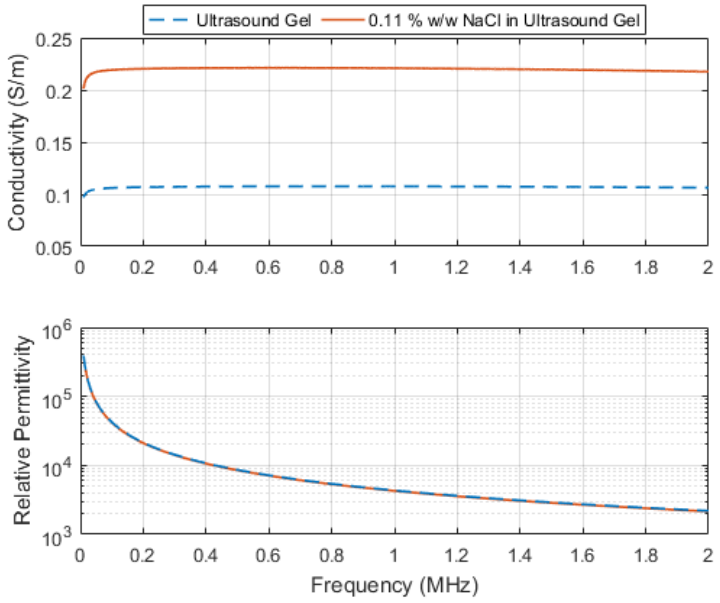


**Figure 4:** The measured conductivity and relative permittivity over frequency of ultrasound gel (product no. 33279, Gima, Italy) and of 0.11 % w/w sodium chloride (NaCl) in ultrasound gel. Each curve consists of 995 points. The small quantity of sodium chloride added to the ultrasound gel has little effect on the relative permittivity. However, conductivity is increased to 0.22 ± 0.001 S $m^{-1}$ over the range of 50-250 kHz, which is within 0.02 S $m^{-1}$ of the calculated target conductivity.

*3.3. Fabrication of the Bladder Phantoms*

We designed solid bladder phantoms out of conductive polyurethane for the volumes 40, 60, 100, 160, 240, 400 ml, each with different dimensions. Isopropanol was added to the conductive polyurethane to increase the conductivity of conductive polyurethane above 0.7 S $m^{-1}$, as detailed in McDermott *et al.*, (2017), which also facilitates the mixing procedure. The composition consisted of 45 % w/w graphite, 3 % w/w carbon black, 2 % v/w isopropanol and the remainder out of equal parts of polyurethane precursors (VytaFlex 20 part A and B, from Smooth-On, Easton, PA, USA). The conductivity of this composition was measured to be 1.895 ± 0.141 S $m^{-1}$ over the selected frequency band of 50-250 kHz. The bladder phantom conductivity fits within the ranges of the reported human urine conductivity found in the literature, as summarised in subsection 2.3.

To create the bladder shapes, hollow half-ellipsoids were formed from the axial, coronal and sagittal radii, outlined in section 2.3, using FreeCad (freecadweb.org). These computer-aided design models were then rapid printed to be used as casts for forming the solid bladder phantoms. The casts are shown in figure 5. For each bladder, the respective 3D prints were filled with the bladder TMM and then joined together, held by the setting polyurethane and gravity. The resulting six bladder phantoms are displayed in figure 5.

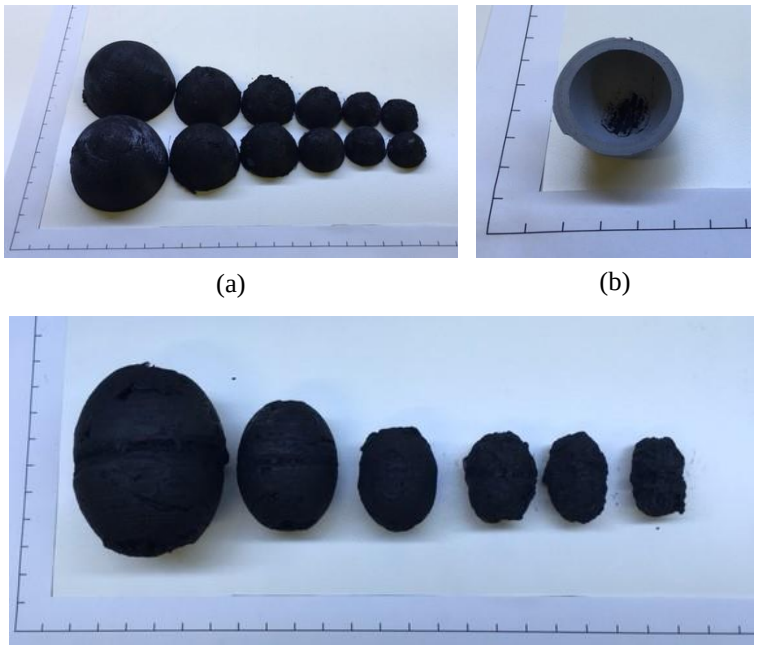

(a) (b)

(c)

**Figure 5:** *(a)* Bladder phantom 3D casts (from left to right) for: 400, 240, 160, 100, 60, and 40 ml. A printed scale is given where each notch marks 1 cm. *(b)* Aerial view of one half of a bladder phantom cast. The two half casts for a particular bladder volume are filled with conductive polyurethane. They are then joined together, held together by the setting conductive polyurethane and gravity. *(c)* The formed bladder phantoms in descending order of volume.

*3.4. Phantom Summary*

An anatomically and conductively accurate pelvic phantom was created for BVM using EI. The phantom consisted of three layers: a realistic boundary; a gel-based internal background material whose conductivity is based on a weighted average of the internal pelvic cavity organs, bone, muscle, and fat; as well as the bladder phantoms representing different bladder volumes. A summary of the properties of each layer is given in table 1.

**Table 1.** Properties of each layer in the modular pelvic phantom.

| | Tissue Mimicking Material | Measured Conductivity | Dimensions |
|---|---|---|---|
| Outer Wall | Conductive Polyurethane w. Graphite and Carbon Black | $0.043 \pm 0.006$ S m$^{-1}$ | 19.5 cm (w)<br>13.3 cm (d)<br>11.2 cm (h) |
| Internal Background Material | Ultrasound Gel and Sodium Chloride | $0.22 \pm 0.001$ S m$^{-1}$ | N/A |
| Bladder Phantoms | Conductive Polyurethane w. Graphite and Carbon Black | $1.895 \pm 0.141$ S m$^{-1}$ | 7.86 mm $\leq r_{Axial} \geq$ 24.43 mm<br>8.15 mm $\leq r_{Coronal} \geq$ 23.36 mm<br>10.90 mm $\leq r_{Sagittal} \geq$ 30.86 mm |

## 4. Experimental & Imaging Results

### *4.1. Experimental Setup*

The Swisstom Pioneer Set (Swisstom.com, Switzerland) was employed to capture data from the pelvic phantom using the settings of 50 kHz frequency, 3 $mA_{peak}$ injection current, and 15 frames s$^{-1}$. A Swisstom electrode belt, 44 cm long, with 32 electrodes, was connected around the pelvic phantom (figure 6). A thin layer of ultrasound gel was applied between the belt and the pelvic phantom to improve contact and maintain a maximum observed contact impedance below 400 Ω. The minimum contact impedance observed was approximately 200 Ω. The pelvic phantom cavity was filled with the background material, 0.11 % w/w sodium chloride in ultrasound gel. The system was allowed to settle for 5 min before recording started. Each 30 second recording was carried out in ascending order of bladder volumes 40, 60, 100, 160, 240, 400 ml and was repeated 3 times. The repeatability was determined for each bladder volume. The maximum standard deviation calculated between sets of frames of a particular bladder volume was 64.376 nV, which indicates that the repeatability of measurements was high. The bladders were supported in the phantom using a thin timber stick and an overhanging stand. The bottom of each bladder phantom was lowered to the same depth in order to mimic the effect of the bladder ascending into the abdominal region as the bladder fills. Each bladder was positioned in the anterior of the phantom, with the centre of the bladder in line with the navel.

**Figure 6:** Illustration of the Swisstom electrode belt fitting on the phantom. The belt is 44 cm long and consists of 32 electrodes. Ultrasound gel was used between the electrodes and pelvic phantom to improve the contact impedance.

### *4.2. Image Reconstruction*

The collected experimental data was processed using the open-source Electrical Impedance Tomography and Diffuse Optical Tomography Reconstruction Software (EIDORS), version 3.9 (Adler *et al.*, 2017). By averaging across each frame entry, the three 30 second recordings for each bladder phantom were combined together to form a single frame. Time-difference image reconstruction was performed using GREIT (Adler, *et al.*, 2009). The 40 ml bladder phantom was considered as the 'empty' bladder state for this experiment and was used as the reference data. A 3D forward model (e.g. 3D finite element model) is recommended for GREIT as 2D forward models do not sufficiently account for the true current distribution within the body (Adler, *et al.*, 2009). Thus, the reconstruction was carried out using a realistic finite element model (FEM) that was based on the same CAD model as the phantom was (Dunne *et al.*, 2017). This mesh was reprocessed using the place electrode method, place_elec_on_surf (Grychtol and

Adler, 2013), in EIDORS. In order to match the experimental electrode-belt setup, the electrodes were angled relative to the horizontal plane at 10° and the place electrode method was enhanced to allow a gap of electrodes at the back of the FEM. The FEM is shown in figure 7 along with the image reconstruction of the 400 ml bladder phantom. This mesh consists of 231,380 nodes and 1,210,800 elements. The quality of the mesh was assessed in terms of the mesh stretch (Tizzard *et al.*, 2005). The mean, standard deviation, minimum and maximum stretch values are: 0.745; 0.086; 0.203; and 0.9911, respectively. These high stretch values indicate a high quality mesh. Further, no stretch values are less than 0.05, which can lead to significant errors in the forward model (Tizzard *et al.*, 2005).

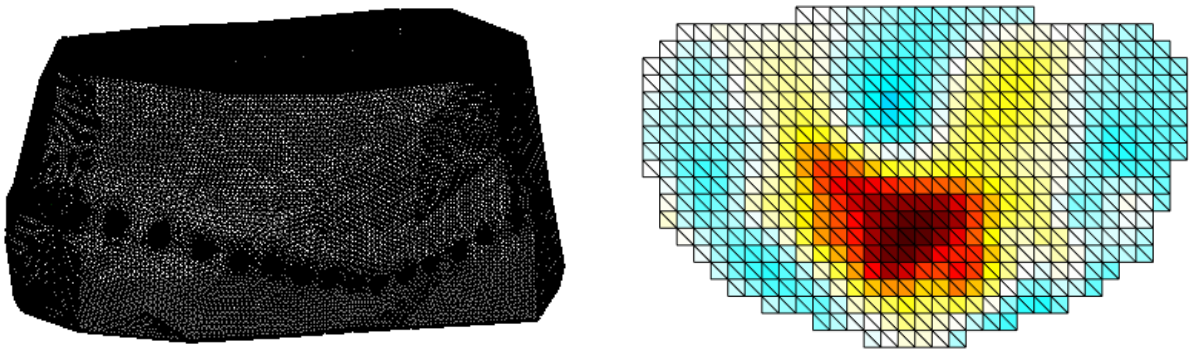

(a) (b)

**Figure 7:** *(a)* Realistic FEM based on the same surface model as the pelvic phantom. The FEM has the electrodes angled at 10° relative to the horizontal and a gap of 60° at the back of the FEM. These modifications were made to match the experimental setup. *(b)* Reconstructed image of the 400 ml bladder. The 40 ml bladder phantom image was used as the reference data. The image amplitudes of the five reconstructed images from 60 ml to 400 ml are [265.74, 1980.5, 5340, 14115, 41509] AU, respectively, indicating that the conductivity of reconstructed data increases with the bladder volume.

The average conductivity index (ACI) has been correlated with bladder volume in previous experimental studies (Li *et al.*, 2015). Therefore, next, we use the ACI to determine the trend from our experiment as bladder volume increases, as shown in figure 8.

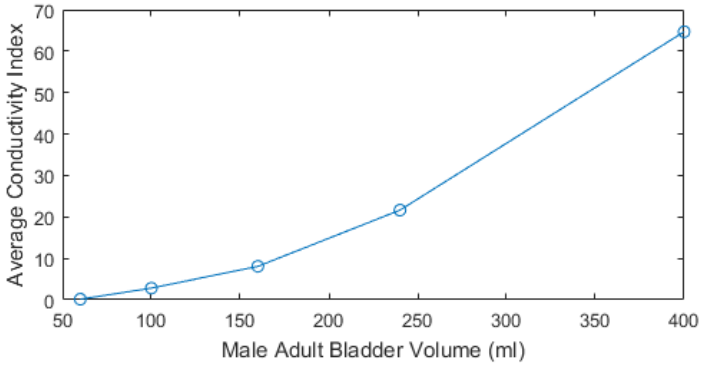


**Figure 8:** The average conductivity index (ACI), determined from image construction, plotted against the male adult bladder volumes that the phantoms represent. The curve of ACI increases monotonically with volume, which is in agreement with the literature (Li *et al.*, 2016).

## 5. Discussion and Conclusion

This paper has presented the first realistic phantom of the pelvic region for bladder volume monitoring using EI. The materials used in developing this modular pelvic phantom are low cost, and are mechanically and conductively stable over time. Significantly, this pelvic phantom will allow experiments to be performed in lab situations to overcome the variables of using EI for bladder volume monitoring such as electrode movement, contact impedance variations, body deformation, and urine conductivity changes. The pelvic phantom will also allow for testing of multi-layer electrodes configurations, electrode type, and size, and internal organ movement, enabling greater scope for experimentation before clinical testing.

Six conductively and proportionally accurate bladders within the pelvic phantom were successfully imaged, as an experimental demonstration of the phantom. A high-quality FEM corresponding to the realistic phantom was employed for the time-difference image reconstruction. The bladders were suspended in the middle of the anterior region of the phantom. This position is correctly captured in the reconstructed images. As expected, the image amplitude increases as the bladder size increases. Each of the bladder volume increments, starting at 20 ml, can be distinguished using the maximum image amplitude or the highly positive correlation between the ACI and the adult bladder volume. The highly positive relationship has been shown previously in Li's *et al.*, (2016) clinical study. However, the amplitude of the ACI curve varies based on bladder conductivity, both between patients and within a patient through their daily diet and health. Therefore, an exact match between curves is unlikely, instead it is the trend of the curve that is of interest.

Overall, this pelvic phantom will support the development and testing of EI bladder monitoring applications. Future work will be undertaken to further improve in order to add the ability for the bladder volume to fill dynamically. For continuous bladder volume experiments, a bladder that is conductively accurate and can expand is desirable. Furthermore, measurements will be performed to examine the impact of parameters such as electrode movement, patient and bladder positioning, and urine conductivity on successful bladder monitoring.

## Acknowledgements

This research was supported by funding from the European Research Council under the European Union's Horizon 2020 Programme/ ERC Grant Agreement BioElecPro n. 637780 and the charity RESPECT and the People Programme (Marie Curie Actions) of the European Union's Seventh Framework Programme (FP7/2007-2013) under REA Grant Agreement no. PCOFUND-GA-2013-608728. The authors would like thank Kite Medical (kitemedical.ie, Kite Medical, Galway, Ireland) for the use of their Swisstom 44 cm electrode belt.

## References

Ackerman M J 1998 The visible human project *Proc. IEEE,* **86** 504–511.

Adler A, *et al.* 2009 GREIT: a unified approach to 2D linear EIT reconstruction of lung images. *Physiol. Meas.* **30** S35–S55.

Adler A, Boyle A, Braun F, Crabb M G, Grychtol B, Lionheart W R B, Tregidgo H F J and Yerworth R 2017 EIDORS Version 3.9 in *Proc.18th Intl. Conf. Biomed. App. of Electrical Imped. Tomography*. Hanover, NH: Zenodo, 63.

Akkus O, Ogus A, Uzunlulu M and Kizilgul M 2012 Evaluation of Skin and Subcutaneous Adipose Tissue Thickness for Optimal Insulin Injection *J. Diabetes Metab.* **3** 1–5.

Chambers, J. (ed.) 2007 The Urinary System in *The Facts On File Encyclopedia of Health and Medicine, Volume 3*. 1st edn. New York: Infobase Publishing, 169–233.

Denniston L C and Baker L E 1975 Measurement of urinary bladder emptying using electrical impedance *Med. Biol. Eng. Comput.* 305–306.

Drake R, Vogl A W, and Mitchell A W 2015 *Gray's anatomy for students*. 3rd edn. Philadelphia, PA: Elsevier.

Dunne E, Porter E, McGinley B and O'Halloran M 2017 Realistic 3D Finite Element Mesh of the Adult Human Pelvis for Electrical Impedance Tomography in *Proc.18th Intl. Conf. Biomed. App. of Electrical Imped. Tomography*. Hanover, NH: Zenodo, 65.

Frerichs I, *et al.* 2016 Chest electrical impedance tomography examination, data analysis, terminology, clinical use and recommendations: consensus statement of the TRanslational EIT developmeNt stuDy group. *Thorax* p. thoraxjnl-2016-208357.

Frerichs I, Hinz J, Herrmann P, Weisser G, Hahn G, Quintel M and Hellige G 2002 Regional lung perfusion as determined by electrical impedance tomography in comparison with electron beam CT imaging *IEEE Trans. Med. Imaging* **21** 646–652.

Gabriel C, Peyman A, and Grant E H 2009 Electrical conductivity of tissue at frequencies below 1 MHz *Phy. Med. Biol.* **54** 4863–4878.

Grimnes S and Martinsen Ø 2008 *Bioimpedance and bioelectricity basics*. Amsterdam: Elsevier.

Grychtol B and Adler A 2013 FEM electrode refinement for electrical impedance tomography in *2013 35th Ann. Intl. Conf. IEEE Eng. Med. Biol. Soc. (EMBC)* 6429–6432.

Hasgall P, Di Gennaro F, Baumgartner C, Neufeld E, Gosselin M, Payne D, Klingenböck A and Kuster N 2015 IT'IS Database for thermal and electromagnetic parameters of biological tissues, Version 3.0.

He W, Ran P, Xu Z, Li B and Li S 2012 A 3D Visualization Method for Bladder Filling Examination Based on EIT *Comp. Math. Methods Med.* Hindawi Publishing Corporation, 1–9.

Hirahara N, Ukimura O, Ushijima S, Yamada Y, Okihara K, Kawauchi A and Miki T 2006 Four-dimensional ultrasonography for dynamic bladder shape visualization and analysis during voiding *J. Ultrasound Med.* **25** 307–13.

Keysight Technologies 2017 *16452A Liquid Test Fixture Operation and Service Manual*. Available at: https://tinyurl.com/ybpsyeo8 (Accessed: 16 August 2017).

Kim C T, Linsenmeyer T, Kim H and Yoon H 1998 Bladder volume measurement with electrical impedance analysis in spinal cord-injured patients *Am. J. Phys. Med. Rehabil.* **77** 498–502.

Krewer F, Morgan F, Jones E, Glavin M and O'Halloran M 2017 Development of A Wearable Microwave Bladder Monitor for the Management and Treatment of Urinary Incontinence in *SPIE Defense+ Security (90770X-90770X)*. International Society for Optics and Photonics.

Leonhardt S, Cordes A, Plewa H, Pikkemaat R, Soljanik I, Moehring K, Gerner H J and Rupp R 2011 Electric impedance tomography for monitoring volume and size of the urinary bladder *Biomed. Tech.* **56** 301–307.

Li J B, Tang C, Dai M, Liu G, Shi X T, Yang B, Xu C H, Fu F, You F S, Tang M X and Dong X Z 2014 A new head phantom with realistic shape and spatially varying skull resistivity distribution *IEEE Trans. Biomed. Eng.* **61** 254–263.

Li R, Gao J, Li Y, Wu J, Zhao Z and Liu Y 2016 Preliminary Study of Assessing Bladder Urinary Volume Using Electrical Impedance Tomography *J. Med. Biol. Eng.* Springer Berlin Heidelberg, **36** 71–79.

Liao W C and Jaw F S 2011 Noninvasive electrical impedance analysis to measure human urinary bladder volume *J. Obstet. Gynaecol Res.* **37** 1071–1075.

Lukacz E S, Sampselle C, Gray M, Macdiarmid S, Rosenberg M, Ellsworth P and Palmer M H 2011 CONSENSUS A healthy bladder : a consensus statement (October) 1026–1036.

Mangnall Y F, Baxter A J, Avill R, Bird, N C, Brown, B H, Barber D C, Seagar A D, Johnson A G and Read N W 1987 Applied potential tomography: a new noninvasive technique for assessing gastric function *Clin. Phys.Physiol. Meas.* **8** 119–129.

McDermott B, McGinley B, Krukiewicz K, Divilly B, Jones M, Biggs M, O'Halloran M and Porter E 2017 Stable Tissue-Mimicking Materials and an Anatomically Realistic, Adjustable Head Phantom for Electrical Impedance Tomography *Biomed. Phys. Eng. Express* 2017 [in press].

Murphy E K, Mahara A, Wu X and Halter R J 2017 Phantom Experiments using Soft-Prior Regularization EIT for Breast Cancer Imaging', *Physiol. Meas.* **38** 1262–1277.

Proença M, Braun F, Solà J, Adler A, Lemay M, Thiran J P and Rimoldi S F 2016 Non-invasive monitoring of pulmonary artery pressure from timing information by EIT: experimental evaluation during induced hypoxia *Physiol. Meas.* **37** 713–726.

Santorelli A, Laforest O, Porter E and Popovi M 2015 Image Classification for a Time-Domain Microwave Radar System: Experiments with Stable Modular Breast Phantoms *9th European Conference on Antennas and Propagation (EuCAP)*.

Schlebusch T, Nienke S, Leonhardt S and Walter M 2014 Bladder volume estimation from electrical impedance tomography, Physiol. Meas. **35** 1813–1823.

Schlebusch T, Orschulik J, Malmivuo J, Leonhardt S, Leonhäuser D, Grosse J, Kowollik M, Kirschner-Hermanns R and Walte M 2014 Impedance ratio method for urine conductivity-invariant estimation of bladder volume *J. Electrical Bioimpedance* **5** 48–54.

Shin, S, Moon, J, Kye, S, Lee, K, Lee, Y S and Kang, H 2017 Continuous Bladder Volume Monitoring System for Wearable Applications in *Proc. 39th Ann. Int. Conf. IEEE EMBS* 4435–4438.

Sperandio M, Guermandi M and Guerrieri R 2012 A Four-Shell Diffusion Phantom of the Head for Electrical Impedance Tomography *IEEE Trans. Biomed. Eng.* **59** 383–389.

Springhouse 2002 *Lippincott Professional Guides: Anatomy & Physiology*. 2nd edn. Lippincott Williams & Wilkins.

Tizzard A, Horesh L, Yerworth R J, Holder D S and Bayford R H 2005 Generating accurate finite element meshes for the forward model of the human head in EIT *Physiol. Meas.* **26** S251–S261.

Zariffa J, Grouza V, Popovic M R and Hassouna M M 2016 A Phase-Based Electrical Plethysmography Approach to Bladder Volume Measurement *Ann. Biomed. Eng.* **44** 1299–1309.

Zhang J, Yang B, Li H, Fu F, Shi X, Dong X and Dai M 2017 A novel 3D-printed head phantom with anatomically realistic geometry and continuously varying skull resistivity distribution for electrical impedance tomography *Sci. Rep.* Springer US **7** 4608.